NJC

PAPER

View Article Online
View Journal | View Issue

Cite this: *New J. Chem.*, 2018, **42**, 11831

Enhanced bactericidal and photocatalytic activities of ZnO nanostructures by changing the cooling route†

Nesrin Horzum, *[a] Mohamed Elhousseini Hilal ‡[bc] and Tuğba Isık ‡[d]

Received 17th April 2018,
Accepted 3rd June 2018

DOI: 10.1039/c8nj01849a

rsc.li/njc

We report on a simple synthesis of ZnO nanowires by calcination of zinc acetate. The effect of calcination temperature and cooling route on the antibacterial and photocatalytic properties is demonstrated by varying the size and surface area of the nanowires. The decrease of the calcination temperature followed by a rapid cooling procedure leads to a smaller size and larger surface area of the nanowires. ZnO nanowires are found to be effective against the growth of *E. coli* at the microgram level. In addition, the photocatalytic activity of the synthesized ZnO nanowires is demonstrated by the successful degradation of the organic dye methylene blue.

Introduction

Water pollution is one of the most significant ecological threats that people face today. By taking the organic and pathogenic pollutants in water sources into consideration, cost-effective and efficient environmental purification methods are required. Antibacterial agents, which are used for the removal of pathogenic pollutants, can be classified as organic and inorganic materials. While organic materials are often less stable at high temperature or pressure, inorganic ones, *i.e.* metal oxides, have promising advantages due to their higher stability compared to organic agents.[1] The nanosized and different shaped structures of metals, metal oxides, and polymers have gained great attention in the last decade.[2–6] Among these materials, metal oxide nanostructures are recognized as the most versatile materials and, in particular, TiO_2, ZnO, Fe_2O_3, and CeO_2 have shown promising results in various applications due to their antibacterial, photocatalytic, electromagnetic, and optical properties.[7–13] These properties contributed to an upsurge of interest in the investigation of synthesis routes that could allow for a better shape and size control.[6,14,15] ZnO is a multifunctional material due to its morphological variety that can be classified into one- (1D), two- (2D), and three-dimensional (3D) structures.[16] While nanorods, nanoneedles, nanowires, and nanobelts have been classified as 1D materials, nanosheets and nanopellets are classified as 2D materials. With regard to 3D structures, snowflakes and cauliflower are examples from nature.[16] In favor of this structural variability, modulating the shape and size can diversify the applications of ZnO materials. There is an extensive range of ZnO application fields, for example as gas sensors, semiconductors, antibacterial agents, and UV-shielding materials, as well as in photocatalysis for wastewater treatment.[17–20]

ZnO powders have been found to exhibit significant antibacterial activity that has been studied extensively with different types of bacteria such as *E. coli* and *S. aureus.* The nontoxic, biologically safe, and biocompatible properties of ZnO nanostructures make them suitable for drug delivery, cosmetics, coatings, and fillings for medical materials.[21] According to Jones *et al.*, ZnO nanoparticles inhibit the growth of pathogenic bacteria significantly when compared to the other metal oxide nanoparticles.[22] Among the various reported parameters, particle size is the most important one that affects antibacterial activity. Padmavathy *et al.* and Yamamoto *et al.* investigated the antibacterial activity of ZnO particles with different particle sizes and both studies proved that antibacterial activity increases with decreasing particle size due to the larger surface area of the particles.[23,24] Applerot *et al.* also confirmed the correlation between the reduction in particle size and the increment in the hydroxyl radical amount and this results in the killing of bacteria.[25]

[a] *İzmir Katip Çelebi University, Engineering Sciences Department, Turkey. E-mail: nesrin.horzum.polat@ikc.edu.tr*
[b] *İzmir Katip Çelebi University, Materials Science and Engineering Department, Turkey*
[c] *Sultan Moulay Sliman University, Chemistry and Environment Department, Morocco*
[d] *İzmir Institute of Technology, Materials Science and Engineering Department, Turkey*

† Electronic supplementary information (ESI) available: Calculated diameter and length of ZnO nanowires, SEM micrograph of zinc acetate, variation of the diameter of ZnO nanowires with respect to fabrication routes, UV-vis absorbance spectra of ZnO nanowires, percentage reduction in bacterial concentrations, UV-visible spectra of MB solutions under UV light irradiation, FTIR spectra of ZnO nanowires, images of antibacterial test solutions to observe turbidity, MIC test images for *E. coli* and *S. aureus* inhibiton. See DOI: 10.1039/c8nj01849a

‡ Mohamed Elhousseini Hilal and Tuğba Isık contributed equally to this study.

On the other hand, a photocatalytic process can potentially be used for environmental remediation, and several semiconductors have been used for photocatalysis over the past few decades. ZnO is recognized as a preferable metal oxide photocatalyst due to its abundance, low cost, photosensitivity, and non-toxic nature.[26] Dyes and pigments are hazardous and can be toxic substances for human beings due to their high discharge into water sources; photocatalysts are used for the degradation of these organic dye pollutants in water sources by an advanced oxidation process (AOP). Pudukudy *et al.* synthesized ZnO structures by various methods (thermal decomposition, surfactant-assisted precipitation–hydrothermal treatment, and solid-state calcination) and investigated the photocatalytic activity of the resulting materials against methylene blue solution.[27–32] Balcha *et al.* synthesized ZnO powders by precipitation and a sol–gel method, and investigated their photocatalytic activity against methylene blue solution.[33] In an alternative method, thermal oxidation was conducted by Atchudan *et al.* ZnO nanoparticle decorated graphene oxide composites were prepared by solvothermal impregnation for the degradation of MB solution.[34] Direct calcination of zinc acetate is a promising ZnO synthesis method with a high yield and without any need for special equipment or organic solvent. Tian *et al.* demonstrated an effective route for the easy and cost-effective synthesis of ZnO photocatalysts by direct calcination of zinc acetate. The obtained ZnO material has been used for the photocatalytic degradation of methyl orange, methylene blue and rhodamine B.[35] Moreover, Pudukudy *et al.* investigated the effect of counter ions on the morphology of ZnO nanostructures and their photocatalytic activity. They reported that the acetate precursor enables the highest photocatalytic activity.[36]

Herein, we revealed a simple route for the synthesis of nano-sized ZnO wires by calcination of zinc acetate at different temperatures and cooling. The ZnO nanowires were cooled by two different methods: free cooling, which is the typical method used after thermal decomposition, while rapid cooling relies on a very short period of cooling down by applying a thermal shock to the sample. ZnO metal oxides prepared at 300 °C showed the smallest size and were implemented for further antibacterial activity and photocatalytic performance applications. The proposed materials show lethal effects even at low antibacterial agent concentrations (0.125 mg mL^{-1}) on *E. coli* growth and they have inhibitory effects on *S. aureus* growth at high concentrations of antibacterial agent. Furthermore, the photocatalytic performance of the ZnO nanowires was investigated by the degradation of MB solutions. The results indicated that the size, antibacterial activity, and photocatalytic performance of the ZnO nanowires were influenced by both calcination temperature and cooling route. This environmentally friendly solvent-free process for ZnO synthesis using a single-source precursor is promising for water purification techniques. The proposed ZnO nanowires could be effectively used not only in dye degradation applications but also for the removal of bacterial pollutants from water sources. This study presents different cooling routes for the synthesis of ZnO nanowires and describes the effect of the resulting morphology on photocatalytic performance and antibacterial activity.

Results and discussion

Structural and morphological characterization of ZnO nanowires

Thermogravimetric analysis (TGA) was performed to study the thermal decomposition of zinc acetate dihydrate and the formation of the ZnO phase. The thermogram in Fig. 1 shows the first weight loss of 16.5% starting from 78 °C to 112 °C, which results due to the evaporation of water components. The second stage below 329 °C reveals a weight loss around 62%, marking the decomposition of anhydrous zinc acetate to ZnO powder. The further weight loss is responsible for the decomposition of the zinc acetate to ZnO powder, indicating that the lowest calcination temperature for ZnO synthesis is around 300 °C. This observation is in good agreement with previous reports.[37,38] The morphology of the zinc acetate precursor was investigated, and it was observed that bulk particles are in non-regular shapes and the size of the particles varies between 160 and 300 μm (Fig. S1, ESI†).

The size and morphology change of the ZnO nanowires was investigated by scanning electron microscopy (SEM). Fig. 2 shows both the effect of calcination temperature and cooling route on the ZnO nanowires. From top to bottom, calcination temperatures are 300 °C, 500 °C, and 700 °C. The left panels of the figure show the ZnO nanowires prepared by free cooling, while the right panel shows the nanowires prepared by rapid cooling. With the increase of the calcination temperature, the diameter and length of the nanowires distinctly vary due to the migration rates of zinc interstitials and vacancies, which are dependent on the growth temperature. When the calcination temperature is high, the thickness of the nanowires becomes larger because of the migration and merging of grain boundaries. At lower temperatures, the nanowires have small diameters, long lengths and sharp structures (Table S1, ESI†). ZnO nanowires can be presumed to have a growth stage that reaches its maximum around 300 °C followed by a shrinking stage at a higher calcination temperature. In addition, the morphology and shape of the ZnO nanowires were affected by not only calcination temperature but also cooling route. A remarkable difference between the left and right panels was observed despite being at the same heating temperature, suggesting different interfacial structures.

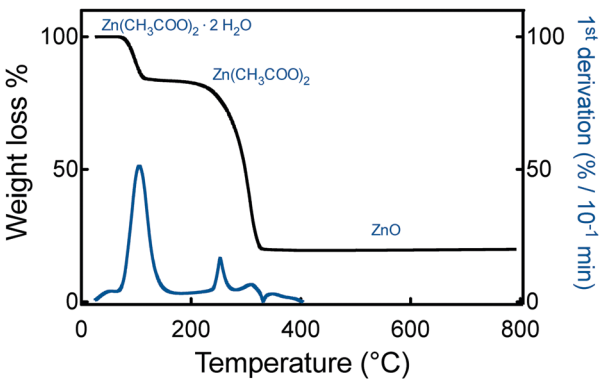

Fig. 1 TGA thermogram of zinc acetate precursor.

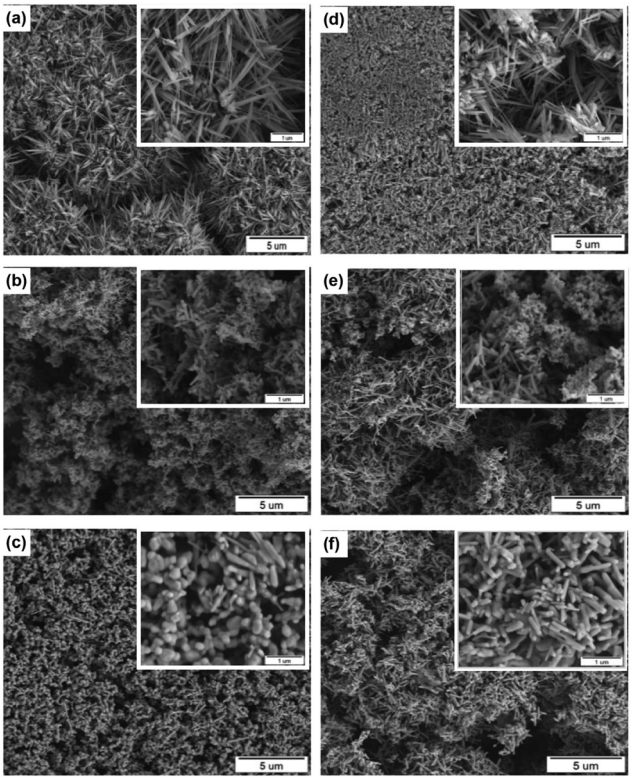

Fig. 2 SEM micrographs of the ZnO nanowires prepared by calcination of $Zn(OAc)_2$ powder at (a and d) 300 °C, (b and e) 500 °C and (c and f) 700 °C. The left panel shows free cooled samples and the right panel shows rapid cooled samples.

The comparison of both cooling routes in terms of ZnO nanowire length is shown in Fig. 3. The rapidly cooled nanowires formed at 300 °C are shorter by 55% than the free cooled ones, suggesting that the nanowires grow significantly during the period of free cooling. However, rapidly cooled nanowires calcined at 500 °C and 700 °C have larger lengths on average, suggesting that shrinkage has been stopped by the very short time of cooling, that is to say that decomposition also mainly occurs during the cooling period. Moreover, the variation of the diameter of the ZnO nanowires was compared with respect to their cooling routes (Fig. S2, ESI†). Initially, the diameter of the rapid cooled nanowires is 15% smaller than the free cooled ones. Afterwards, the diameter of the rapid cooled ones became nearly 13% thicker than the free cooled ones at both 500 °C and 700 °C. The reason for this thickening is probably shrinking of the nanowires at high temperatures.

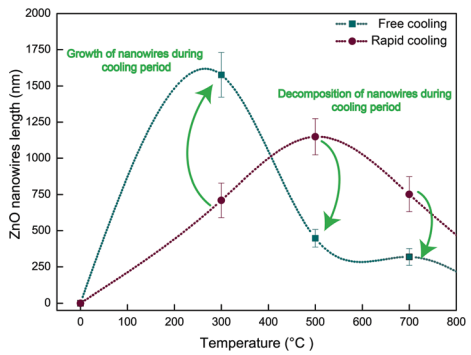

Fig. 3 Comparison of the length of the ZnO nanowires obtained by free cooling and rapid cooling. (The length of the nanowires was calculated from SEM micrographs by using ImageJ software.)

The X-ray diffraction (XRD) patterns of the samples, prepared by free cooling (FC) and rapid cooling (RC), at different calcination temperatures are shown in Fig. 4. The XRD reflections can be indexed using the Inorganic Crystal Structure Database (reference code: 03-065-3411) with a hexagonal crystal structure. Both FC and RC samples, which were calcined at different temperatures, have the same series of peaks at 31.82°, 34.48°, 36.32°, 47.58°, 56.65°, 62.94°, 66.41°, 68.02°, and 69.14° indexed subsequently as (100), (002), (101), (102), (110), (103), (200), (112), and (201), which reveal the presence of the ZnO wurtzite crystalline structure without impurities. Moreover, the absence of any shifts among all diffractograms of the nanowires disclaims the occurrence of any lattice expansion and/or shrinkage. With the increase in calcination temperature, the intensity of the diffraction peaks increases, indicating the strengthened ZnO phase. Furthermore, it is worth mentioning that the diffraction signals of the RC samples (Fig. 4b) are slightly more intense than those of the FC samples (Fig. 4a), likely due to the exposure of the hot calcined powder to air during rapid cooling, which further promotes the formation of the oxide phase.

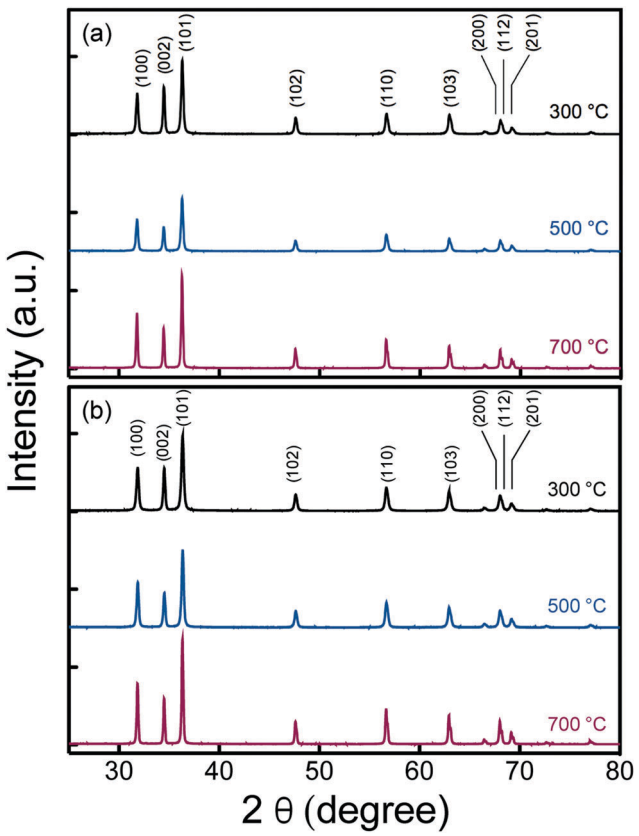

Fig. 4 XRD patterns of the zinc acetate powder calcined at 300, 500 or 700 °C followed by (a) free cooling or (b) rapid cooling.

Table 1 Average crystallite size and BET surface area of the synthesized ZnO nanowires

	Average crystallite size (nm)		BET surface area (m^2 g^{-1})	
Temperature of calcination (°C)	Free cooled ZnO	Rapid cooled ZnO	Free cooled ZnO	Rapid cooled ZnO
300	34	9	15	35
500	34	33	7	19
700	45	32	6	21

Average crystallite sizes of ZnO nanowires were roughly estimated by the Scherrer equation employing the (101) reflection (Eqn (1)) and the results are presented in Table 1,

$$D\ (\mathrm{nm}) = \frac{K\lambda\ (\mathrm{nm})}{\beta(rd)\cos\theta} \quad (1)$$

where D is the crystallite size, K is the Scherrer constant (0.9), λ is the wavelength of Cu (Kα) radiation (0.154056 nm) and β is the full width at half maximum (FWHM). Both the FC and RC nanowires show an increment in the crystallite size directly proportional to an increase in temperature. It can be clearly seen that particle morphology is influenced by temperature, which promotes the enlargement of grain boundaries and consequently the particle size increases. Because the reduction in the overall surface energy is a driving force for the enlargement of the grain boundary, the particle size increases as a function of temperature. Calcination facilitates the movement of atoms through the mass transport mechanism that results in grain growth.[39] On the other hand, the comparison between the FC and RC nanowires demonstrates that crystallite sizes of the FC ones are slightly higher, because there is a sufficient cooling time to gather up and form larger grains for the FC samples.

The BET results emphasize a reasonable reduction of the surface area due to the increase of the calcination temperature, as demonstrated by Zheng *et al.* the increase of ZnO crystallite size impacts the BET surface area negatively.[40] Moreover, the rapidly cooled samples have a remarkably larger surface area than their free cooled counterparts because the samples that cool faster result in smaller crystals compared to the samples cooled slowly.[41] The optical properties of the ZnO nanowires were also studied by UV-vis spectroscopy (Fig. S3, ESI†). The absorption wavelength of the free cooled samples is larger than that of the rapidly cooled ones so there is an increase in the band gap energy of the samples. The band gap energy was calculated to be $E_g = 1240/\lambda$, where E_g is the band gap energy in eV and λ is the wavelength in nanometers. E_g values of the free cooled and rapidly cooled samples at 300 °C were calculated to be 3.33 and 3.36 eV, respectively. The lower band gap energies of the free cooling samples could be attributed to the larger crystallite size of these samples in Table 1.[32,42]

Antibacterial activity of the ZnO nanowires

The antibacterial activity of the ZnO nanowires was examined using Gram-negative bacteria (*E. coli*) and Gram-positive bacteria (*S. aureus*) as models. On the whole, the antibacterial mechanism of metal oxide powders could be affected by several parameters, which could be the eluted cations from the powder, the pH of the medium, the generation of reactive oxygen species (ROS) from the surface of metal oxide, and the mechanical destruction of the cell membrane.[24] However, there is a massive effect of particle size on the antibacterial activity of the nanoparticles. According to literature arguments, the generation of H_2O_2 from the surface increases with decreasing particle size due to the increase in surface area, *i.e.* the number of metal oxide particles per unit volume increases. Thus, the ZnO nanowires with the smallest size and the highest surface area, FC@300 and RC@300, were chosen for antibacterial activity tests. The antibacterial activity of the ZnO nanowires involves a multicomponent mechanism. When UV or visible light irradiates the surface of the ZnO nanoparticles, electron–hole pairs are created and the holes split the H_2O molecules into OH^- and H^+. Then, the dissolved O_2 molecules are converted to radical anions, react with H^+ and form HO_2 radicals followed by collision of the electrons with these radicals, and the generation of HO_2^- anions. Finally, HO_2^- anions react with H^+ ions to produce H_2O_2.[39,43] The produced H_2O_2 could penetrate the cell membrane and achieve bactericidal activity. For the evaluation of the ZnO powder concentration on the antibacterial effect, the minimum inhibitory concentrations (MICs) of FC@300 and RC@300 samples were measured. MIC shows the endpoint, where no turbidity can be detected with respect to the control samples. Fig. 5 shows the logarithmic growth of *E. coli* and *S. aureus* bacteria in the presence of different concentrations of ZnO nanowires. The increment in the concentration of ZnO nanowires inhibits the bacterial growth of both bacteria. The percentage of *E. coli* reduction was found to be ≥99% for FC@300 and RC@300 samples even at very low concentrations (0.125 mg mL^{-1}) (Fig. S4, ESI†).

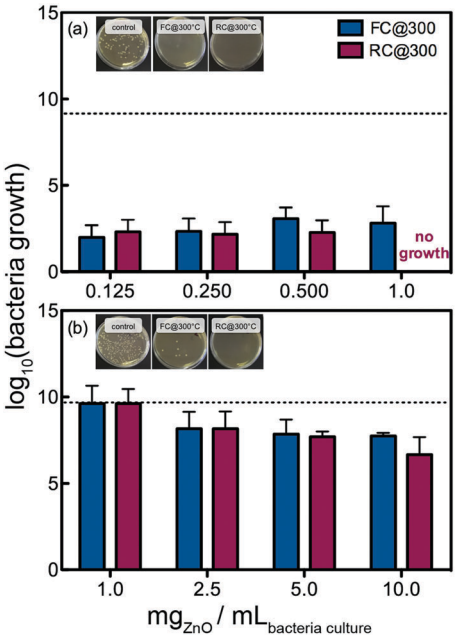

Fig. 5 Bacterial growth of (a) *E. coli* and (b) *S. aureus* against different concentrations of the FC@300 and RC@300 nanowires. The dotted lines show the logarithmic bacterial concentration in the control samples.

Also, the MIC of the RC@300 sample was found to be 1.0 mg mL^{-1} for *E. coli* inhibition. In the presence of FC@300 nanowires, there is a higher amount of bacterial growth compared to that of RC@300 (Fig. 5a). Because the influence of particle size, namely surface area, is effective in the inhibition of bacterial growth, the RC@300 nanowires cause a larger amount of bacterial death due to their larger surface areas. The same interpretation could be made for *S. aureus* growth that the RC@300 nanowires show the inhibition of a larger amount of bacteria when compared to FC@300 (Fig. 5b).

Based on the results obtained from MIC tests, it can be suggested that in comparison with *S. aureus* inhibition, the influence of ZnO nanowires on *E. coli* growth was stronger due to the structural differences of the bacteria. On the cell surface of *E. coli*, there are thin layers of lipid A, lipopolysaccharide, and peptidoglycan while the cell surface of *S. aureus* only consists of peptidoglycan layers.[24] Sawai *et al.* investigated the relation between H_2O_2 generation from ZnO nanoparticles and their antibacterial activity, and suggested that H_2O_2 is one of the primary factors contributing to the antibacterial activity.[44] The ZnO nanowires increase the membrane permeability through the bacterial cell during their deposition of ROS around the surface of the cell membrane. Then, internalization of nanowires in the cell membrane induces the generation of H_2O_2, which can oxidize DNA, enzyme, and protein in the bacterial cells. Therefore, the differences in antibacterial activities of *E. coli* and *S. aureus* probably come from the different sensitivities towards H_2O_2. Fig. 5b shows the growth of *S. aureus* in the presence of different concentrations of the ZnO nanowires. In this case, MIC could not be calculated because even at very high concentrations of antibacterial agents, there is no complete reduction in *S. aureus* bacteria. Also, *S. aureus* reduction was found to be $\geq$99% only for a 10.0 mg mL^{-1} concentration of the RC@300 nanowires (Fig. S3, ESI†). It can be concluded that the proposed nanowires are promising candidates only for *E. coli* reduction and a rapid cooling procedure has a significant effect on the inhibition of bacterial growth.

Photocatalytic performance of the ZnO nanowires

In principle, valence band electrons in semiconductors are excited to the conduction band and leave holes (h^+) when the material is exposed to a light energy. While the holes generate hydroxyl radicals by oxidizing H_2O and OH^-, excited electrons are captured by oxygen and produce anionic radicals, which are capable of oxidizing organic pollutants.[45–48] The synthesized ZnO nanowires were used as a photocatalyst for the degradation of MB under simple UV-light irradiation and the degradation of MB was examined using UV-vis spectroscopy. In general, MB displays a blue color in water and absorbs in the visible region at 612 and 664 nm. Fig. 6a shows the time-dependent UV-vis spectra of MB in the presence of RC@500 ZnO nanowires under UV-light irradiation. The absorbance of the MB solution at 664 nm gradually decreased with irradiation time in the presence of ZnO nanowires. Along with the spectral changes, the MB solution changed from blue to nearly colorless after 50 min of irradiation of the RC@500 ZnO nanowires.

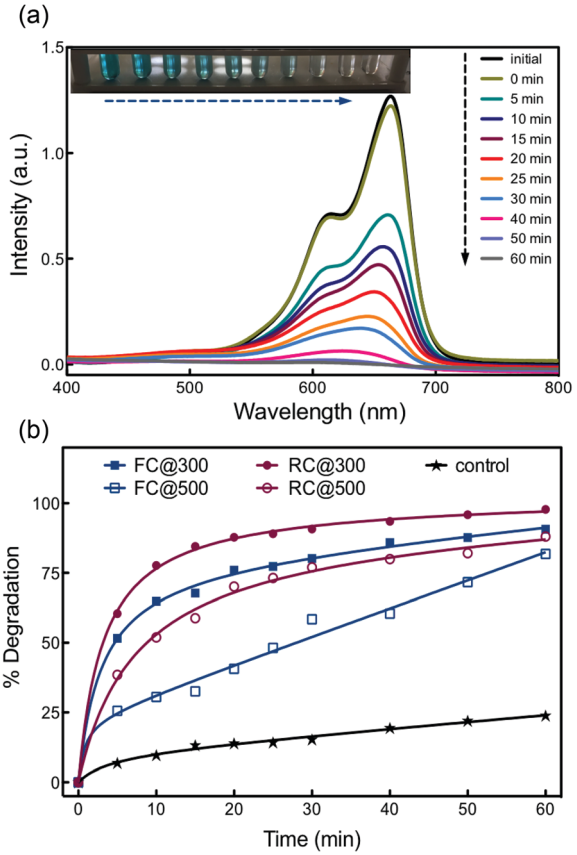

Fig. 6 (a) UV-visible spectrum of MB solution under UV light irradiation in the presence of RC@500 ZnO nanowires. Inset: Colour change of MB adsorption over 60 min. (b) Percentage degradation of MB dye under UV radiation as a function of time using different ZnO nanowires. (R^2, correlation coefficient, values are 0.9906, 0.9981, 0.9992, 0.9878, and 0.9959 for control, FC@300, RC@300, FC@500, and RC@500, respectively.)

The plots of percentage degradation of the MB dye under UV irradiation as a function of time are shown in Fig. 6b. The percentage degradation of ZnO nanowires was calculated by using the time-dependent UV visible spectra of nanowires (Fig. S5, ESI†). In the absence of ZnO nanowires, the MB dye was quite stable and its degradation was negligible under UV light irradiation. The photocatalytic degradation of the as-synthesized nanowires showed similar photocatalytic activities such that their degradation percentages first increased with the increase in irradiation time and reached a plateau value after a while. When the percentage degradation results of free cooled and rapidly cooled nanowires were compared, it could be obviously seen that the rapidly cooled samples have higher photocatalytic activity than the free cooled samples for both calcination temperatures. Also, the highest percentage of degradation was achieved by RC@300 nanowires (88%, 20 min) due to their larger surface area, while FC@500 (41%, 20 min) nanowires exhibited the lowest photocatalytic activity because of unstable degradation behavior. The increase in the photocatalytic activity with the increase in the surface area is probably due to the increased number of active sites on the photocatalytic surface.[33] The smaller size was obtained by rapid cooling, where the

carriers reach the surface to participate in photocatalytic activity. The increase in the crystallite size enhances the probability of charge recombination outside the barrier region.[49] Thus, rapid cooling is more preferred over free cooling, as far as high photocatalytic activity is concerned.

Conclusions

One-dimensional nanostructured zinc oxide (ZnO) wires were synthesized through several heat treatments combined with two different cooling routes. The effect of cooling route on pore size and volume as well as surface area leads to the conclusion that rapid cooling seems promising giving strong microproperties that could be useful in many fields. The synthesized ZnO nanowires were implemented for antibacterial activity and photocatalytic performance applications. The proposed materials show lethal effects even at low antibacterial agent concentrations (0.125 mg mL^{-1}) on *E. coli* growth, and they have an inhibitory effect on *S. aureus* growth at a high concentration (10.0 mg mL^{-1}) of antibacterial agent. Furthermore, the photocatalytic performance of the ZnO nanowires was investigated by the degradation of methylene blue solutions. Similarly, the rapidly cooled samples exhibit higher photocatalytic activity compared to the free cooled samples. The higher percentage of methylene blue degradation was achieved by RC@300 nanowires (88%, 20 min). We show the possibility to improve the properties of ZnO nanowires by thermal shocking aiming to employ it as a powerful alternative gathering cost-effectiveness, accessibility, and efficiency for several domains.

Experimental

Fabrication of the ZnO nanowires

ZnO nanowires were synthesized by the thermal decomposition of zinc acetate dihydrate ($Zn(CH_3COO)_2{\cdot}2H_2O$, Aldrich, 99.9%) at 300, 500, and 700 °C for 12 h with a rate of 4 °C min^{-1}. 0.5 g of the metal salt precursor in an alumina crucible was placed in a muffle oven (Protherm furnaces, PLF/20/27, Turkey) to produce ZnO nanowires. To investigate the effect of cooling route on the structure and formation of ZnO, two different routes were applied: free cooling that takes place slowly by keeping the sample in the oven, and rapid cooling by partially immersing the sample crucible in a cold-water bath to cool it down faster. While the nanowires prepared by free cooling were abbreviated as FC@300, FC@500, and FC@700; rapid cooling samples were abbreviated as RC@300, RC@500, and RC@700.

Structural and morphological characterization methods

ZnO nanowires were covered by 2 nm of gold using a Q150RES coater to increase their conductivity, and the morphology of the nanowires was investigated by using SEM (Carl Zeiss 300VP, Germany). The length and diameter of nanowires were measured using image processing software, ImageJ. The crystalline phase, crystallite size, and purity of the ZnO nanostructures were investigated using a Philips X'Pert Pro X-ray diffractometer (Philips X'Pert Pro, Eindhoven, The Netherlands). A copper anode was used under 45 kV and 40 mA of current in the theta–theta configuration with a scanning range from 5° to 80° and at a time per step of 15.24 s. In order to obtain the thermogram of $Zn(OAc)_2$, thermogravimetric analysis (TGA) was performed using a TA Instruments (SDT Q600 V20.9 Build 20), depositing the samples on alumina substrates and heating in a nitrogen atmosphere with a ramp of 10 °C min^{-1} to 800 °C. The Brunauer–Emmett–Teller methodology (BET, Micromeritics 3Flex) was used to calculate the N_2 adsorption–desorption isotherms of the resulting materials at 77 K in order to determine the surface area characteristics and pore sizes. Fourier transform infrared (FTIR) spectra were recorded using a Thermo Scientific Nicolet iS5 spectrometer with a spectral resolution of 4 cm^{-1}. Attenuated total reflection (ATR) infrared measurements of the calcined samples were also performed (Fig. S6, ESI†).

Antibacterial activity tests

The antibacterial activity of the ZnO nanowires was tested against Gram-negative *E. coli* (ATCC 25922) and Gram-positive *S. aureus* (RSKK 1009 strain) bacteria. Both bacterial strains were obtained from Environmental Research Centre and Biotechnology, and Bioengineering Research and Application Centre of IZTECH, İzmir, Turkey. A typical antibacterial procedure was as follows: the bacterial cultures were grown overnight on Nutrient Broth (NB) and Tryptic Soy Broth (TSB) for *E. coli* and *S. aureus*, respectively. The day after, these cultures were transferred into a test tube and optical density of cultures was adjusted to the 0.5 McFarland standard (bacterial concentration: 2.5×10^7 and 3.4×10^7 CFU mL^{-1} for *E. coli* and *S. aureus*, respectively) by adding peptone water (DEN-1 Densitometer, Riga, Latvia). Then, the bacterial cultures were diluted with NB and TSB to 10^5 CFU mL^{-1} bacterial concentrations for *E. coli* and *S. aureus*, respectively. To evaluate the antibacterial activity, *E. coli* and *S. aureus* were grown in NB and TSB media, respectively, with different concentrations of ZnO nanowires (FC@300 and RC@300). After the preliminary studies, the required concentrations for these tests were determined to be between 0.125 to 1.0 mg mL^{-1} and 1.0 to 10.0 mg mL^{-1} for *E. coli* and *S. aureus*, respectively. Also, the control samples were prepared for both *E. coli* and *S. aureus* without adding any ZnO nanowires. For each sample and bacterial culture, three repetitive experiments were done and the bacterial cultures were cultivated in an incubation shaker at 37 °C and 200 rpm for 24 h. Then, the turbidity of bacteria was initially deduced by turbidity visualization (Fig. S7, ESI†). Each of the incubated bacterial cultures were diluted at a ratio of 1 : 10 with peptone water. This procedure was continued up to the 4th dilution for *E. coli* and the 6th dilution for *S. aureus*. (This procedure was applied for easy quantification of bacteria growth.) Then, 100 μL of each sample (stock and diluted ones) was transferred on to the NB and TSB agar plates for *E. coli* and *S. aureus*, respectively. The plates were allowed to grow for 24 h at 37 °C in an incubator (Fig. S8 and S9, ESI†). Then, viable bacteria were counted and expressed as CFU mL^{-1}. The antibacterial activity of the nanowires was defined as follows:

$$\text{Antibacterial activity } (\%) = \left(\frac{N_0 - N}{N_0}\right) \times 100 \qquad (2)$$

where N_0 denotes the number of CFU before adding the antibacterial agent and N denotes the number of CFU after the addition of the antibacterial agent.

Photocatalytic activity

The photocatalytic activity of ZnO nanowires was examined employing a model reaction of Methylene Blue (MB) under UV irradiation. MB (AppliChem) solution was prepared at a concentration of 0.02 mM at neutral pH. Then, 2.5 mg of each catalyst (FC@300 and RC@300) was added in 50 mL of MB solution and stirred for 20 minutes in the dark to complete the adsorption and desorption equilibrium between the photocatalyst and the dye. Afterwards, the solutions were irradiated with a 300 W UV lamp (Osram Ultra Vitalux, Germany) for 20 minutes, and the UV source was kept at a distance of 10 cm above the beaker. The photocatalytic degradation of the MB dye for both the initial concentration and irradiated samples was determined using a UV-vis spectrophotometer (SHIMADZU, UV 2550, Japan) through color disappearance. The percentage degradation of methylene blue was calculated by the following equation:

$$\text{Degradation } (\%) = \left(\frac{(A_0 - A_t)}{A_0}\right) \times 100 \qquad (3)$$

Conflicts of interest

There are no conflicts of interest to declare.

Acknowledgements

The authors thank E. Culcular for his assistance with SEM at IKCU Central Research Laboratory. The Center for Materials Research and the Biotechnology & Bioengineering Research and Application Center at Iztech are also acknowledged for XRD and antimicrobial studies, respectively.

References

1 K. Anagnostakos, P. Hitzler, D. Pape, D. Kohn and J. Kelm, *Acta Orthop.*, 2008, **79**, 302–307.
2 A. P. Alivisatos, *Science*, 1996, **271**, 933–937.
3 C. Burda, X. B. Chen, R. Narayanan and M. A. El-Sayed, *Chem. Rev.*, 2005, **105**, 1025–1102.
4 Y. Cui, Q. Q. Wei, H. K. Park and C. M. Lieber, *Science*, 2001, **293**, 1289–1292.
5 X. W. Lou, L. A. Archer and Z. C. Yang, *Adv. Mater.*, 2008, **20**, 3987–4019.
6 Y. N. Xia, P. D. Yang, Y. G. Sun, Y. Y. Wu, B. Mayers, B. Gates, Y. D. Yin, F. Kim and Y. Q. Yan, *Adv. Mater.*, 2003, **15**, 353–389.
7 A. Azam, A. S. Ahmed, M. Oves, M. S. Khan, S. S. Habib and A. Memic, *Int. J. Nanomed.*, 2012, **7**, 6003–6009.
8 N. Horzum, M. Mari, M. Wagner, G. Fortunato, A. M. Popa, M. M. Demir, K. Landfester, D. Crespy and R. Munoz-Espi, *RSC Adv.*, 2015, **5**, 37340–37345.
9 N. Horzum, R. Munoz-Espi, G. Glasser, M. M. Demir, K. Landfester and D. Crespy, *ACS Appl. Mater. Interfaces*, 2012, **4**, 6338–6345.
10 N. Horzum, D. Tascioglu, S. Okur and M. M. Demir, *Talanta*, 2011, **85**, 1105–1111.
11 H. B. Ma, P. L. Williams and S. A. Diamond, *Environ. Pollut.*, 2013, **172**, 76–85.
12 V. Shah, S. Shah, H. Shah, F. J. Rispoli, K. T. McDonnell, S. Workeneh, A. Karakoti, A. Kumar and S. Seal, *PLoS One*, 2012, 7.
13 W. R. Xu, W. J. Xie, X. Q. Huang, X. Chen, N. Huang, X. Wang and J. Liu, *Food Chem.*, 2017, **221**, 267–277.
14 M. H. Huang, S. Mao, H. Feick, H. Q. Yan, Y. Y. Wu, H. Kind, E. Weber, R. Russo and P. D. Yang, *Science*, 2001, **292**, 1897–1899.
15 N. Satoh, T. Nakashima, K. Kamikura and K. Yamamoto, *Nat. Nanotechnol.*, 2008, **3**, 106–111.
16 E. de Lucas-Gil, J. F. Fernandez and F. Rubio-Marcos, *Mater. Des.*, 2017, **134**, 188–195.
17 Y. Li, T. Lv, F. X. Zhao, Y. L. Zou, X. X. Lian, Q. J. Zhou, H. P. Liu and D. M. An, *Mater. Technol.*, 2016, **31**, 192–196.
18 E. A. Meulenkamp, *J. Phys. Chem. B*, 1998, **102**, 5566–5572.
19 E. J. Tang, G. X. Cheng, X. S. Pang, X. L. Ma and F. B. Xing, *Colloid Polym. Sci.*, 2006, **284**, 422–428.
20 M. N. Xiong, G. X. Gu, B. You and L. M. Wu, *J. Appl. Polym. Sci.*, 2003, **90**, 1923–1931.
21 N. L. Rosi and C. A. Mirkin, *Chem. Rev.*, 2005, **105**, 1547–1562.
22 N. Jones, B. Ray, K. T. Ranjit and A. C. Manna, *FEMS Microbiol. Lett.*, 2008, **279**, 71–76.
23 N. Padmavathy and R. Vijayaraghavan, *Sci. Technol. Adv. Mater.*, 2008, **9**, 035004.
24 O. Yamamoto, *Int. J. Inorg. Mater.*, 2001, **3**, 643–646.
25 G. Applerot, A. Lipovsky, R. Dror, N. Perkas, Y. Nitzan, R. Lubart and A. Gedanken, *Adv. Funct. Mater.*, 2009, **19**, 842–852.
26 M. R. Hoffmann, S. T. Martin, W. Y. Choi and D. W. Bahnemann, *Chem. Rev.*, 1995, **95**, 69–96.
27 S. Prabhu, M. Pudukudy, S. Sohila, S. Harish, M. Navaneethan, D. Navaneethan, R. Ramesh and Y. Hayakawa, *Opt. Mater.*, 2018, **79**, 186–195.
28 M. Pudukudy, Z. Yaakob, R. Rajendran and T. Kandaramath, *React. Kinet., Mech. Catal.*, 2014, **112**, 527–542.
29 M. Pudukudy and Z. Yaakob, *Superlattices Microstruct.*, 2013, **63**, 47–57.
30 M. Pudukudy and Z. Yaakob, *Appl. Surf. Sci.*, 2014, **292**, 520–530.
31 M. Pudukudy and Z. Yaakob, *J. Cluster Sci.*, 2014, 26.
32 M. Pudukudy, A. Hetieqa and Z. Yaakob, *Appl. Surf. Sci.*, 2014, **319**, 221–229.
33 A. Balcha, O. P. Yadav and T. Dey, *Environ. Sci. Pollut. Res.*, 2016, **23**, 25485–25493.
34 R. Atchudan, T. Edison, S. Perumal, D. Karthikeyan and Y. R. Lee, *J. Photochem. Photobiol., B*, 2016, **162**, 500–510.
35 C. G. Tian, Q. Zhang, A. P. Wu, M. J. Jiang, Z. L. Liang, B. J. Jiang and H. G. Fu, *Chem. Commun.*, 2012, **48**, 2858–2860.
36 M. Pudukudy and Z. Yaakob, *Solid State Sci.*, 2014, **30**, 78–88.

37 M. Singh, G. Palazzo, G. Romanazzi, G. P. Suranna, N. Ditaranto, C. Di Franco, M. V. Santacroce, M. Y. Mulla, M. Magliulo, K. Manoli and L. Torsi, *Faraday Discuss.*, 2014, **174**, 383–398.
38 B. S. Ong, C. S. Li, Y. N. Li, Y. L. Wu and R. Loutfy, *J. Am. Chem. Soc.*, 2007, **129**, 2750–2751.
39 X. Y. Bai, L. L. Li, H. Y. Liu, L. F. Tan, T. L. Liu and X. W. Meng, *ACS Appl. Mater. Interfaces*, 2015, **7**, 1308–1317.
40 Y. H. Zheng, C. Q. Chen, Y. Y. Zhan, X. Y. Lin, Q. Zheng, K. M. Wei, J. F. Zhu and Y. J. Zhu, *Inorg. Chem.*, 2007, **46**, 6675–6682.
41 W. D. Callister and D. G. Rethwisch, *Materials Science and Engineering: An Introduction*, John Wiley and Sons, Inc., USA, 8 edn, 2011.
42 A. J. Reddy, M. K. Kokila, H. Nagabhushana, J. L. Rao, C. Shivakumara, B. M. Nagabhushana and R. P. S. Chakradhar, *Spectrochim. Acta, Part A*, 2011, **81**, 53–58.
43 A. Stankovic, S. Dimitrijevic and D. Uskokovic, *Colloids Surf., B*, 2013, **102**, 21–28.
44 J. Sawai, S. Shoji, H. Igarashi, A. Hashimoto, T. Kokugan, M. Shimizu and H. Kojima, *J. Ferment. Bioeng.*, 1998, **86**, 521–522.
45 N. Serpone, *Sol. Energy Mater. Sol. Cells*, 1995, **38**, 369–379.
46 L. L. He, Z. F. Tong, Z. H. Wang, M. Chen, N. Huang and W. Zhang, *J. Colloid Interface Sci.*, 2018, **509**, 448–456.
47 A. L. Linsebigler, G. Q. Lu and J. T. Yates, *Chem. Rev.*, 1995, **95**, 735–758.
48 S. S. Soni, M. J. Henderson, J. F. Bardeau and A. Gibaud, *Adv. Mater.*, 2008, **20**, 1493–1498.
49 L. M. F. Arias, A. A. Duran, D. Cardona, E. Camps, M. E. Gomez and G. Zambrano, in *Workshop on Oxide Materials 2014: Novel Multifunctional Properties*, ed. M. E. Gomez and W. Lopera, 2015, vol. 614.

